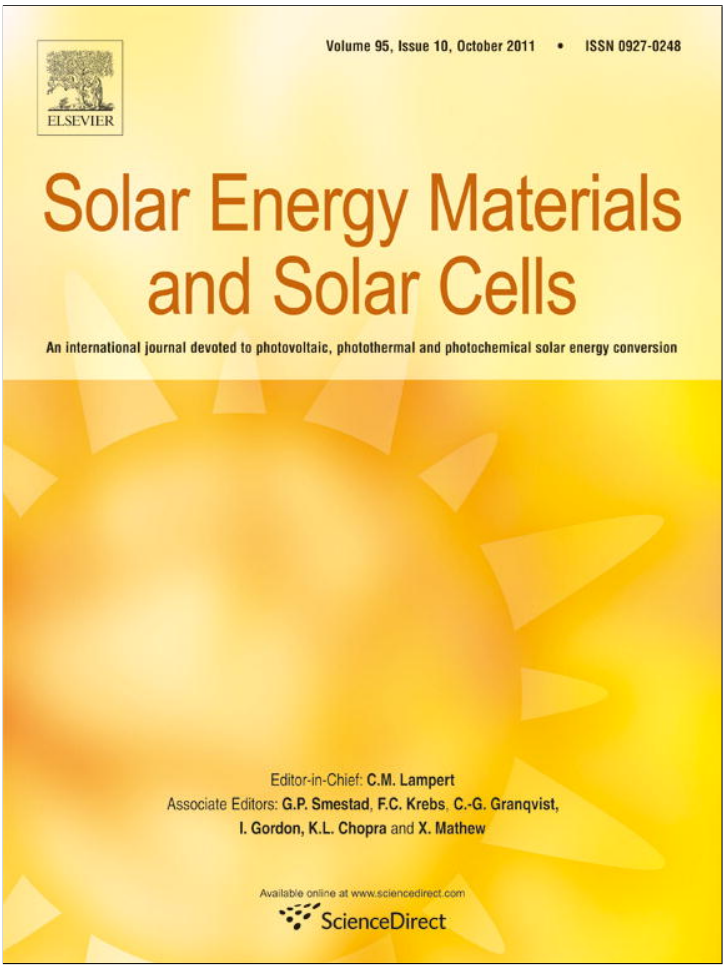

Solar Energy Materials & Solar Cells 95 (2011) 2816–2822

Contents lists available at ScienceDirect

Solar Energy Materials & Solar Cells

journal homepage: www.elsevier.com/locate/solmat

Over 30% transparency large area inverted organic solar array by spray

Jason E. Lewis, Evan Lafalce, Patrick Toglia, Xiaomei Jiang*

Department of Physics, University of South Florida Tampa, FL 33620, USA

ARTICLE INFO

Article history:
Received 1 February 2011
Received in revised form
14 May 2011
Accepted 16 May 2011
Available online 24 June 2011

Keywords:
Organic solar array
Photovoltaic
Inverted geometry
Spray
Conjugated polymer

ABSTRACT

We report the fabrication and characterization of large scale inverted organic solar array fabricated by all-spray process. The inverted polymer solar cell geometry consists of four layers, in the order of ITO–Cs_2CO_3–(P3HT:PCBM)–modified PEDPT:PSS, on a glass substrate. With semitransparent PEDPT:PSS as anode, the encapsulated solar array shows more than 30% transmission in the visible–near IR range. Optimization of device is done by thermal annealing, and the optimal annealing conditions are shown to be different in single-cell test device and the multiple-cell array. Solar illumination has been demonstrated to improve solar array efficiency up to 250%. Device efficiency of 1.80% was observed with the array under AM1.5 irradiance. Our preliminary data have shown that the performance enhancement under illumination only happens with sprayed devices, not devices made by spin coating. This means that solar cells made with our spray-on technique performs better under sunlight, which is beneficial for solar energy application.

Published by Elsevier B.V.

1. Introduction

Organic photovoltaic (OPV) devices based on π-conjugated polymers have been intensively studied following the discovery of fast charge transfer between polymer and carbon C_{60} [1–9]. The photovoltaic process in OPV first starts from the absorption of light mainly by the polymer, followed by the formation of excitons. The exciton then migrates to and dissociates at the interface of donor (polymer)/acceptor (fullerene). Separated electrons and holes travel to opposite electrodes via hopping, and are collected at the electrodes, resulting in an open circuit voltage (V_{oc}). Upon connection of electrodes, a photocurrent (short circuit current, I_{sc}) is created.

These polymeric OPV holds promise for potential cost-effective photovoltaics since it is solution processable. Large area OPVs have been demonstrated using printing [10–12], spin-coating and laser scribing [13–15], and roller painting [16]. ITO, a transparent conductor, is commonly used as hole collecting electrode (anode) in OPV, and a normal geometry OPV starts from ITO anode, with the electron accepting electrode (cathode) usually a low work function metal such as aluminum or calcium, being added via thermal evaporation process.

There are two different approaches in inverted geometry. One approach is completely ITO-free, using a wrap-through method by Zimmermann et.al. [17], or the use of a Kapton foil and an Aluminum/Chromium bi-layer system as electron contact [18], and the formation of a bottom electrode comprising silver nanoparticles on a 130 μm thick polyethyleneternaphthalate (PEN) substrate by Krebs et.al. [19]. Another approach is to add an electron transport layer onto ITO to make it function as cathode. Inverted geometry OPVs in which the device was first built from modified ITO as cathode have been studied both in single cells [20–23] and solar modules [10].

OPV single cell utilizing spray technique has been previously reported [24–26]. However, all these works involve either the use of high vacuum deposition, and/or spin-coating process. For the inverted solar array fabricated by spray, ours is the first of its kind. Comparing with conventional technology based on spin-coating and using metal as a cathode contact, which greatly limits transparency of solar cells and posts difficulty for large scale manufacturing, the new spray technology solves these two problems simultaneously. A thin film organic solar array is fabricated employing this layer-by-layer spray technique onto desired substrates (can be rigid as well as flexible). This technology eliminates the need for high vacuum, high temperature, low production rate and high-cost manufacturing associated with current silicon and in-organic thin film photovoltaic products. Furthermore, this technology could be used on any type of substrate including cloth and plastic.

Traditionally, solar modules made from silicon are installed on rooftops of buildings. However, it can be a hassle for the installation since these solar modules are heavy and brittle. In addition, rooftop area is limited compared with the window area in normal building, and even less in skyscrapers. However, in order for solar cells to be compatible with windows, transparency is the first to be considered. The metal contacts used in traditional solar

* Corresponding author.
E-mail address: xjiang@usf.edu (X. Jiang).

0927-0248/$ - see front matter Published by Elsevier B.V.
doi:10.1016/j.solmat.2011.05.037

modules are visibility-blocking and has to be replaced. OPV modules fabricated by other large scale manufacturing techniques such as printing [10,16] and spin-coating [14,15] have been demonstrated; however, all these still involve the use of metal in certain way.

The literature results have shown PCE as high as 0.42% for a solution-based all-spray device [27], which was opaque. In this report, we start with a semitransparent single-cell test device, which has PCE of 1.2% under AM1.5 solar irradiance, and further demonstrate the development of an all-spray technique to fabricate large scale solar array on a $4'' \times 4''$ substrate consisting of 50 cells with total active area of 30 cm^2. The overall transmittance of the finished solar array is over 30%, and the device power conversion efficiency (PCE) of as high as 1.80% was achieved under constant AM1.5 solar irradiance.

2. Experimental

Poly(3-hexylthiophene) (P3HT) with regioregularity over 99% was purchased from Riekie Metals, with an average molecular weight of 42 K. 6,6-phenyl C61 butyric acid methyl ester (PCBM) with 99.5% purity was purchased from Nano-C. The original aqueous poly (3,4) ethylenedioxythiophene:poly-styrenesulfonate (PEDOT:PSS) Baytron 500 and 750 were obtained from H. C. Starck. The pre-cut $4'' \times 4''$ ITO glass substrates with a nominal sheet resistance of 4–10 Ω/square and Corning® low alkaline earth boro-aluminosilicate glass were obtained from Delta Technology, Inc. Cs_2CO_3 was purchased from Aldrich. All masks for spray are custom made by Towne Technologies, Inc. The airbrush sets for spray was purchased from ACE hardware.

ITO with desired pattern was prepared by the standard photolithography method and cleaned following the procedure described elsewhere [28]. Cs_2CO_3 solution in 2-ethoxyethanol with a concentration of 2 mg/ml was sprayed onto the clean ITO substrate through a custom made shadow mask with an airbrush using N_2 as the carrier gas. The finished substrate is annealed at 150 °C for 10 min inside the N_2 glovebox (MBraun MOD-01).

The active layer solution is made by mixing P3HT and PCBM with a weight ratio of 1:1 in dichlorobenzene at 20 mg/ml and stirred on a hot plate for 48 h at 60°C prior to spraying. Active layer was sprayed onto the Cs_2CO_3 coated substrate using an airbrush, resulting in a layer thickness of about 200–300 nm. The device is then left to dry in the antechamber under vacuum for at least 12 h.

The original aqueous poly (3,4) ethylenedioxythiophene:poly-styrenesulfonate (PEDOT:PSS) was diluted and filtered out through a 0.45 μm filter. This filtered solution of PEDOT:PSS is mixed with 5 vol% of dimethylsulfoxide to increase conductivity [27]. This modified PEDOT:PSS (m-PEDOT) is then sprayed onto the substrate using a custom made spray mask.

The finished device is then put into high vacuum (10^{-6} Torr) for 1 h. This step was shown to improve the device performance with sprayed active layer [27]. The final device is then annealed at various conditions (see results section) and encapsulated using a UV-cured encapsulant (EPO-TEK OG142-12) from Epoxy Technology.

The current–voltage (*I–V*) characterization of the solar array was performed with a Newport 1.6 KW solar simulator under AM1.5 irradiance of 100 mW/cm^2. No spectral mismatch with the standard solar spectrum was corrected in the power conversion efficiency (PCE) calculation. The incident photon converted electron (IPCE), or the external quantum efficiency (EQE), of the device was measured using 250 W tungsten halogen lamp coupled with a monochromator (Newport Oriel Cornerstone 1/4 m). The photocurrent was detected by a UV enhanced silicon detector connected with a Keithley 2000 multimeter. The transmission spectrum of active layer was performed on the same optical setup.

3. Results/discussion

3.1. Characteristics of test device by spray

In order to have a good reference point for the multi-cell array, we started with an inverted single-cell test device, which consists of four identical small cells (4 mm^2) on a $1'' \times 1''$ substrate (Fig. 1). The test device was fabricated using the same procedure described in the Experimental section, with m-PEDOT 500 as anode.

ITO normally has a work function of ~4.9 eV. The function of ITO in traditional OPV device is as anode. There have been previous reports on tuning the work function of ITO by adding an electron transport layer such as ZnO [21], TiO_2 [20], PEO [23] and Cs_2CO_3 [20] in inverted OPV single cells. In this work, we chose to use Cs_2CO_3 for its economic cost and easy handling. By spin coating a solution of 2-ethoxyethanol with 0.2% Cs_2CO_3 at 5000 rpm for 60 s, a very thin layer (~10 Å) of Cs_2CO_3 is formed over the ITO. It was reported that a dipole layer would be created between Cs_2CO_3 and ITO. The dipole moment helped to reduce the work function of ITO, allowing ITO to serve as the cathode [20].

Fig. 2 shows how the Cs_2CO_3 layer affects the performance of the inverted cell. The control cell without Cs_2CO_3 (black solid line) performed almost like a resistor and had negligible V_{oc} (0.03 V).

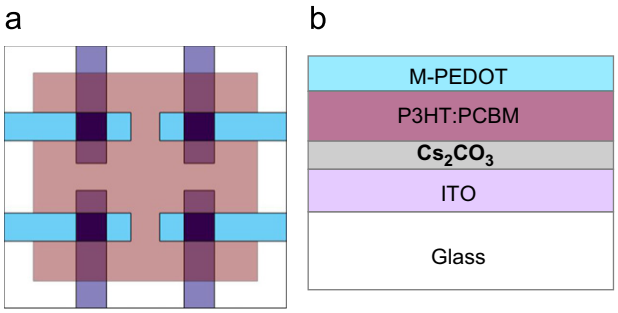

Fig. 1. Device structure of an inverted test cell. (a) Top view; (b) side view.

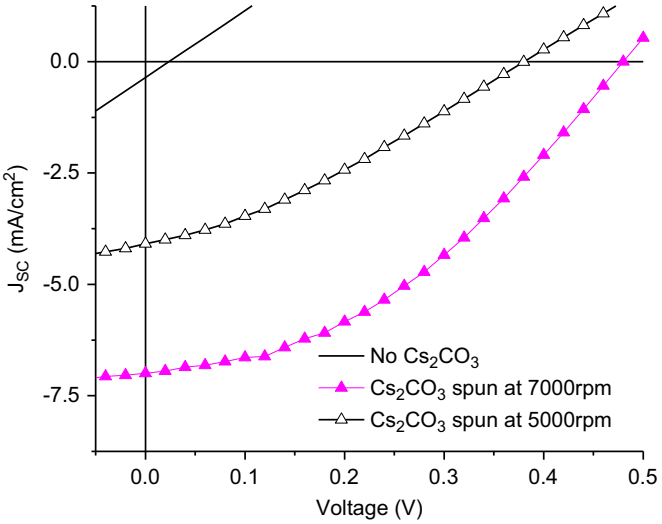

Fig. 2. *I–V* characteristics of three test cells: without Cs_2CO_3 layer (black solid line), and with Cs_2CO_3 layer at different thicknesses (black line with empty triangle and magenta line with filled triangle). (For interpretation of the references to color in this figure legend, the reader is referred to the web version of this article).

The difference between our result and the work in Ref. [23] can be explained by the use of an electron transport layer to alleviate non-ohmic contact with the cathode (PEDOT in this case) in their work. For a better controlled thickness, Cs_2CO_3 was spin-coated onto the cleaned ITO substrate in these devices. As shown in Fig. 2, the optimal thickness of Cs_2CO_3 layer was achieved at a spin rate of 5000 rpm. At higher rate of 7000 rpm, the device was less efficient owing to the fact of a discontinuous Cs_2CO_3 layer. We found out that the optimal thickness is between 10 and 15 Å measured by AFM topography.

Previous report showed Cs_2CO_3 can lower the ITO work function to as low as 3.3 eV [20]. In order to get an estimate of the effective work function of ITO/Cs_2CO_3 cathode, we have fabricated a control device with 100 nm aluminum deposited on glass substrate as cathode, with the active layer and m-PEDOT layer fabricated the same way as in ITO/Cs_2CO_3 cathode configuration. Since aluminum is not transparent, the *I–V* in both devices were measured by illumination from m-PEDOT side. V_{oc} of such control device was 0.24 V, whereas V_{oc} of the ITO/Cs_2CO_3 cathode device (magenta line in Fig. 2) was 0.36 V measured under the same illumination condition. Since aluminum has work function of 4.2 eV, this means in our case, the effective work function of ITO/Cs_2CO_3 is close to 4.1 eV.

Fig. 3 shows how the thickness of m-PEDOT affects its transmittance (a) and sheet resistance (b). Transmittance was measured using a 250 W tungsten halogen lamp coupled with a monochromator (Newport Oriel Cornerstone 1/4 m). The sheet resistance of m-PEDOT was measured using a standard four-point probe measurement [29,30]. These two parameters (transmittance and sheet resistance) are important to assess the feasibility of m-PEDOT to be used as a replacement contact for the conventional metal contact. ITO was chosen as a reference for comparison. At a thickness of about 100 nm, the transmittance of m-PEDOT is about 80%, comparable with ITO. As expected, the resistance decreases as thickness increases, which is consistent with the bulk model. The trade-off between transparency and resistance is another important fabrication parameter. The current array was fabricated with thickness of about 600 nm, which has moderate resistance of 70 Ω/square, and transmittance about 50%. Shown in Fig. 4 was a comparison between transmission spectra of the active layer (P3HT:PCBM, 200 nm) and m-PEDOT anode of 600 nm. The total transmittance over the spectra range shown decreases from 73% to 31% after spraying on the m-PEDOT anode.

Annealing has shown to be the most important factor to improve organic solar cell performance [4,5]. Fig. 5 shows the comparison of current–voltage (*I–V*) and incident photon converted electron (IPCE) or external quantum efficiency (EQE) between three inverted test cells at different annealing conditions: 1-step annealing at either 120 °C (red filled circle), or 160 °C (black filled square) for 10 min; 2-step annealing at 120 °C for 10 min, followed by high vacuum for 1 h and annealing at 160 °C for 10 min. The rationale behind choosing such annealing conditions was to experiment both annealing temperature and the thermal profile. Fig. 5a shows that 1-step annealing at 120 °C gives the best result in test cell, with V_{oc}=0.48 V, I_{sc}=0.23 mA, FF=0.44, and a power conversion efficiency (PCE) of 1.2% under AM1.5 solar illumination with intensity 100 mW/cm^2. The second annealing step at 160 °C worsens the device performance, mainly due to unfavorable change of film morphology, which was confirmed in AFM images in Fig. 6. The PCE of 1-step annealing at 160 °C was in between 1-step annealing at 120 °C and 2-step annealing, yet the device has the worst FF. Table 1 listed the details of the *I–V* characteristics of these three test cells. Further investigation of thermal profile with finer steps than 40 °C is ongoing to determine the optimal annealing conditions.

In Fig. 5b, IPCE measurement shows 2-step annealing was worse than 1-step annealing, which was consistent with the *I–V* measurements in Fig. 6a. There seems to be some inconsistency

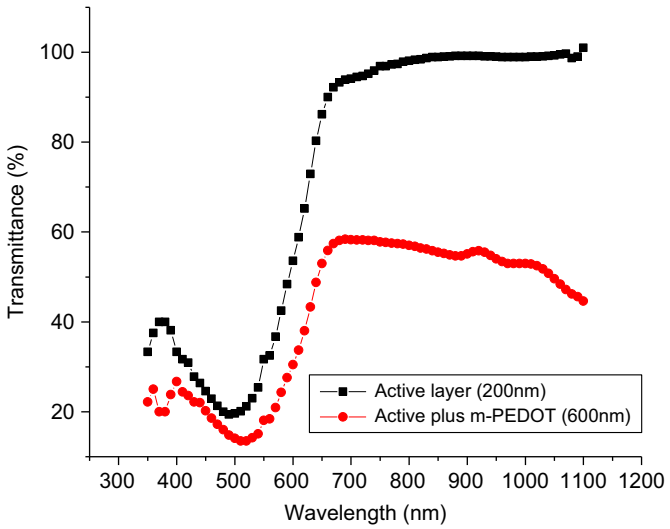

Fig. 4. Transmission spectra of an active layer (P3HT:PCBM) of 200 nm (black line with filled square), and with a m-PEDOT:PSS layer of 600 nm (red line with filled circle). (For interpretation of the references to color in this figure legend, the reader is referred to the web version of this article).

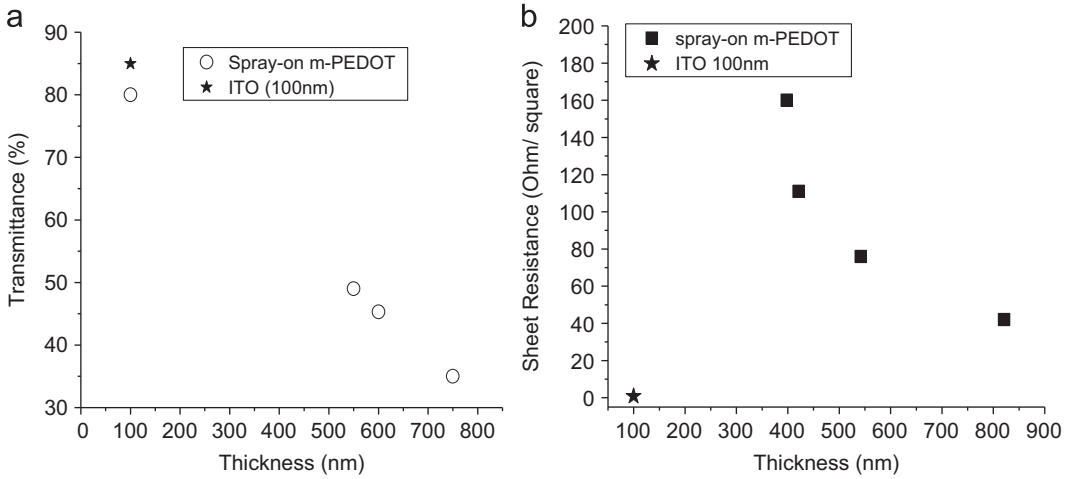

Fig. 3. Comparison of (a) transmittance and (b) sheet resistance between ITO and the spray-on anode (modified PEDOT:PSS, or m-PEDOT) with different thicknesses.

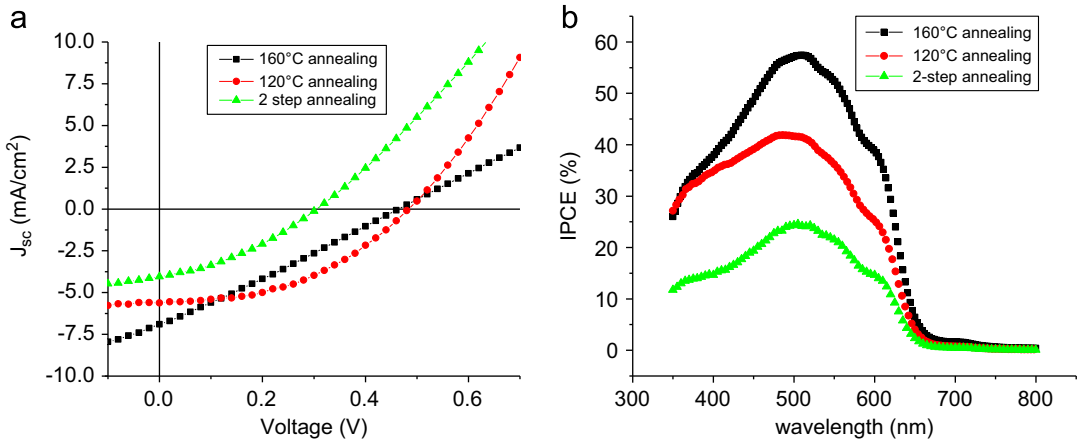

Fig. 5. (a) *I–V* characteristics of three test cells measured with AM1.5 solar illumination under various annealing conditions: 1-step annealing at 120 °C (red filled circle), or 160 °C (black filled square), and 2-step annealing (green filled triangle); (b) IPCE of the same devices measured under tungsten lamp illumination. (For interpretation of the references to color in this figure legend, the reader is referred to the web version of this article).

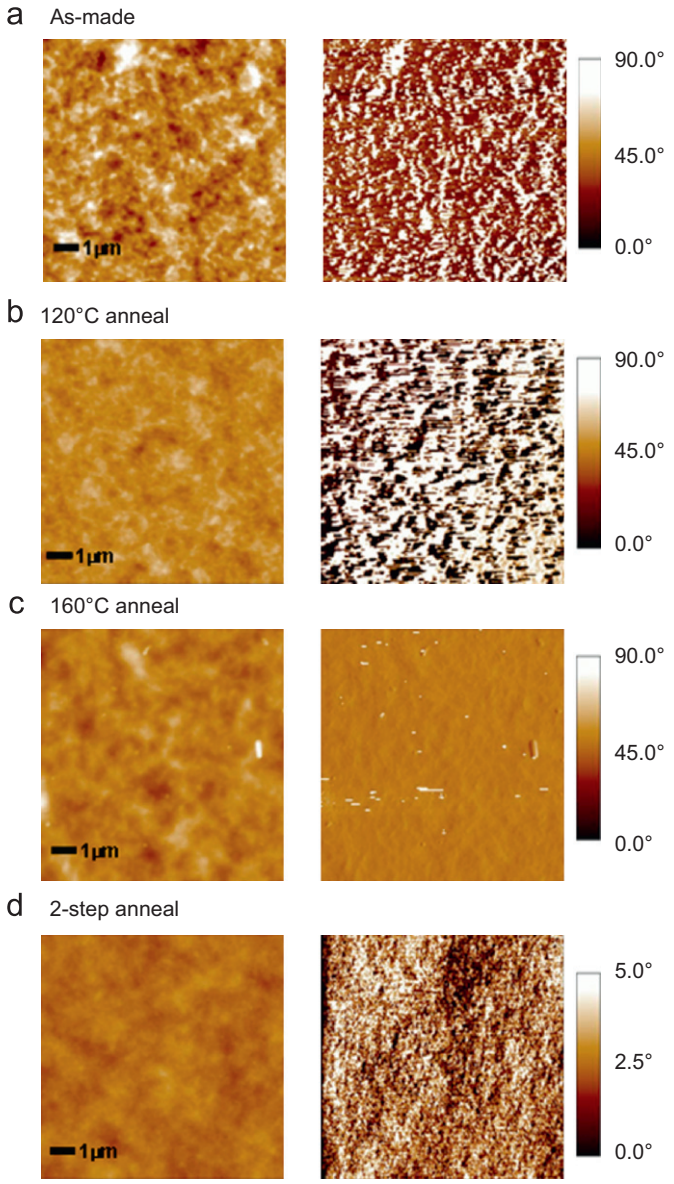

Fig. 6. AFM images of 4 test cells under various annealing conditions as shown in figure. As-made cell, (b) 1-step annealing at 120 °C, (c) at 160 °C and (d) 2-step annealing. Left panel shows topography, and right panel the phase image.

Table 1
Test cell *I–V* characteristics comparison at various annealing conditions.

Test cell number	I_{sc} (mA)	V_{oc} (V)	*FF*	η (%)	Annealing condition
1	0.28	0.48	0.26	0.86	160 °C 10 min
2	**0.23**	**0.48**	**0.44**	**1.2**	120 °C 10 min
3	0.16	0.30	0.35	0.43	2-step

between PCE and IPCE for the cells annealed at 160 and 120 °C: the cell annealed at 160 °C has higher IPCE yet lower PCE than that at 120 °C. IPCE measurement was done under illumination from Tungsten lamp, whereas *I–V* was done under solar simulator, which has a different spectrum than that of the tungsten lamp. Nevertheless, the integration of IPCE should be proportional to I_{sc}. The device made by 1-step annealing at 160 °C, though having smaller power conversion efficiency, actually has larger I_{sc} (0.28 mA) than the one at 120 °C (0.23 mA). The ratio between integral of IPCE at 160 °C vs. 120 °C is about 1.3, and the ratio of I_{sc} of the same devices was 1.2. The slight discrepancy might also come from the fact that the cells behave differently under strong (IV) and weak (IPCE) illuminations. Usually bi-molecular (BM) recombination sets in under high light intensity (solar simulator) [4], meaning the cell, which has more prominent BM recombination, will perform poorer with high intensity illumination such as that from the solar simulator. It might be that the cell annealed at 160 °C was affected by BM recombination more than the cell annealed at 120 °C, due to more traps associated with rougher morphology (see Fig. 6) serving as recombination centers. The same mechanism can also be applied to explain the larger difference in IPCE of device annealed at 160 °C and by 2-step annealing than that of their I_{sc} in Fig. 5. Further investigation of this discrepancy is under study.

Fig. 6 shows the AFM images [topography (left panel) and phase (right panel)] of four test cells at different annealing conditions. 1-step annealing at 120 °C (b) showed the improved film roughness and the best phase segregation of P3HT and PCBM, which explains why the device performance was the best (Fig. 5). Device by 2-step annealing has the smoothest film, however, the phase segregation was much less distinct. This indicates that P3HT chains and PCBM molecules are penetrating through each other more after the second annealing at 160 °C, and form much smaller nano-domains, which are favorable for charge transport between the domains [31]. However, recombination of photo-generated carriers might be enhanced due to the lack of separate

pathways for electron sand holes, and that was why the device after 2-step annealing performed worse than after the 1st annealing at 120 °C (Fig. 5). 1-step annealing at higher temperature of 160 °C results in the roughest film (even rougher than the as-made device), and the P3HT phase and PCBM phase are hardly distinguishable. This rough film also further affects the interface between active layer and m-PEDOT, resulting in poor FF of the device (Fig. 5).

3.2. Large area solar array by spray

Fig. 7a shows the device architecture of a finished solar array with inverted structure. The array consists of 50 individual cells each has an active area of 60 mm^2. The array was configured with 10 cells in series in one row to increase the voltage, and five rows in parallel connection to increase the current. Fig. 7b presents the cross section of a single cell and how the series connection was made with the neighboring cell. These arrays either have m-PEDOT 750 or m-PEDOT 500 as semitransparent anode.

Fig. 8 shows the *I–V* of four arrays under different annealing conditions measured with AM1.5 solar illumination. It is clear that 1-step annealing at low temperature (120 °C) gives the worst result, 2-step annealing showed improved *I–V* characteristics (V_{oc}, J_{sc}, FF and PCE) after the second high temperature annealing

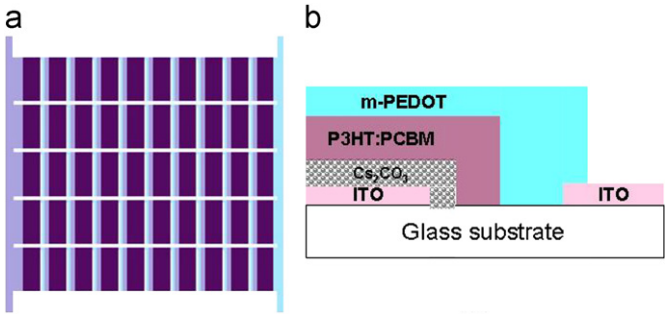

Fig. 7. Device architecture of an inverted solar array. (a) Top view; (b) side view showing series connection.

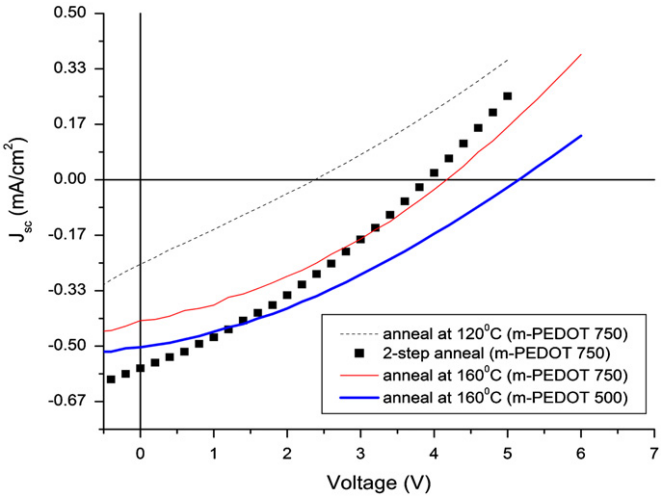

Fig. 8. *I–V* characteristics of 4 inverted spray-on solar arrays measured with AM1.5 solar illumination under various annealing conditions: 1-step annealing at 120 °C (dashed line), or 160 °C (red thin line), and 2-step annealing (black filled square). These 3 arrays use m-PEDOT 750 as anode. The 4th array (thick blue line) uses m-PEDOT 500 as anode and was annealed at 160 °C. (For interpretation of the references to color in this figure legend, the reader is referred to the web version of this article).

Table 2
Array *I–V* characteristics comparison at various annealing conditions.

Array number	I_{sc} (mA)	V_{oc} (V)	*FF*	η (%)	Annealing condition	m-PEDOT
1	17.0	3.9	0.30	0.68	2-step	750
2	11.5	4.0	0.39	0.62	2-step	750
3	6.30	2.8	0.37	0.22	2-step	750
4	13.0	4.0	0.33	0.56	160 °C 10 min	750
5	15.0	5.2	0.33	0.86	160 °C 10 min	500
6	12.0	5.8	0.30	0.70	160 °C 10 min	500
7	11.1	5.2	0.35	0.67	160 °C 10 min	500

at 160 °C. 1-step annealing at high temperature (160 °C) gives the best V_{oc}, and 2-step annealing yields the highest J_{sc}. In terms of anode, m-PEDOT 500 seems to give higher V_{oc} than PEDOT 750 (see Table 2 for more array results). However, there is not much difference of PCE between 2-step annealing and 1-step annealing at 160 °C, which is in contrast with the result of the test device (Fig. 5). We think the annealing duration is probably too short for the array, since it has much larger area and contains much more materials. Further investigation of interplay between annealing temperature, duration and thermal profile is ongoing to find the optimal device fabrication conditions.

We have observed a very interesting phenomenon, which we call as 'photo annealing' (Fig. 9). Under constant illumination from the solar simulator, a sudden change of *I–V* characteristics occurs after certain amount of time, which is device dependent, ranging from 10 min to several hours. The device shown in Fig. 9 takes about 15 min, and reaches maximum PCE after 2.5 h under illumination. The drastic change is mostly I_{sc}, which is more than double from 17 to 35 mA after 2.5 h. The change of V_{oc} was marginal from 4.0 to 4.2 V. The maximum PCE of the array was 1.80%. Table 3 listed the changes of other *I–V* characteristics.

Furthermore, this sudden increase of I_{sc} is also accompanied by a characteristic 'wiggles' on the *I–V* curve. We propose several mechanisms to explain the above observations. The first mechanism is due to optical interference causing re-distribution of light intensity within the active layer. The sealant epoxy was heated and softened, resulting in the change of the distance between encapsulating glass and the device, causing less optical loss. As a consequence, the short circuit current I_{sc} increases. This mechanism was supported by the inset of Fig. 9, which shows the fast decay of a spray-on test cell without encapsulation. Encapsulation also helps to minimize oxidization and slow down the decay of organic solar cell efficiency.

The second mechanism is that photo annealing of active layer improves morphology and has cured some of the weak points (burned out shorts), thus improves I_{sc} and FF. It might be due to the fact that the porosity of sprayed film is much larger than the spin-coated film, and polymer chains have much more loose arrangement in sprayed device, with the heat from solar illumination, the polymer chains relax more and the film nanomorphology was improved, with possibly PCBM penetrating into the voids between polymer chains and causing better phase segregation [32]. This effect is similar to thermal annealing performed on hot plate. As temperature drops down, the polymer chains go back to its original configuration, and the *I–V* curve is back to its original one, manifesting certain kind of thermal hysteresis.

The third mechanism is due to the thermal activation of the previous deeply trapped carriers (i.e., polarons), which results in increased photocurrent at higher temperature [33,34]. The wiggles indicate the non-uniformity of the film morphology, and the overall boost of device performance is the result of the free-up of previously trapped charges in the active layers.

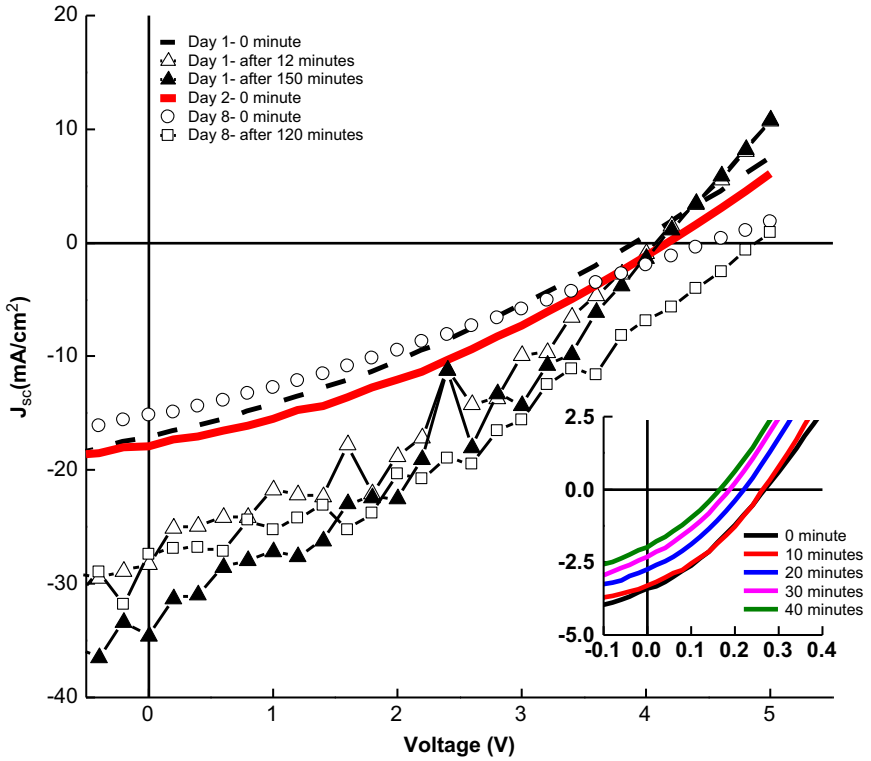

Fig. 9. Improvement of *I–V* characteristics of an inverted solar array under continuous AM1.5 solar illumination. The first measurement (dashed black line) was done right after the array was fabricated and encapsulated. The inset shows the time dependence of *I–V* characteristics of a spray-on test cell (without encapsulation).

Table 3
Change of array *I–V* characteristics under solar illumination.

Time	I_{sc} (mA)	V_{oc} (V)	*FF*	η (%)
Day 1				
–0 min	17	4.0	0.30	0.68
–12 min	28	4.2	0.35	1.40
–150 min	35	4.2	0.37	1.80
Day 2				
–0 min	18	4.2	0.35	0.88
Day 8				
–0 min	15	4.4	0.29	0.64
–120 min	27	4.8	0.38	1.68

This observation is against the conventional picture of organic solar cell, which normally shows degradation under solar illumination [35]. We also found out that the performance enhancement under illumination only happened with sprayed devices, not the device made by spin coating. This means that solar cells made with our spray-on technique performs better under sunlight, which is beneficial for solar energy application. The methods, data and results presented in this report are based on our early work. Current research includes enhancements to architecture, improvements in power production and ongoing study of photo annealing dynamics and solar array lifetime. Promising early results have warranted further research, targeting optimal performance of the solar array in field operations.

4. Conclusions

We have demonstrated large area organic array fabricated by an all-spray technique. Cs_2CO_3 was chosen to reduce ITO work function close to 4.0 eV to be utilized as cathode. The fully encapsulated $4'' \times 4''$ array has over 30% transparency and can produce as high as 1.80% of power conversion efficiency (PCE) under constant illumination of simulated sunlight. Thermal annealing has proven to be essential to improve device PCE, and the optimal annealing conditions are not the same with small single cell and large solar array consisting of 50 cells. Systematic study of optical, electronic and morphologic properties of the device reveals the influence of nanomorphology over device power conversion efficiency. Moreover, our discovery of photo annealing, i.e., more than 2-fold increase of solar cell PCE under solar irradiance and with hysteresis pattern, is in contrary to the normal understanding of organic solar cell degradation under sunlight. The fact that photo annealing was only observed with sprayed solar cell or arrays places an advantageous solution to our technique for large scale, low-cost solution-based solar energy applications. Ongoing research includes identifying optimal parameters for the production of a high efficiency solar array.

Acknowledgements

This work was supported by New Energy Technologies Inc. and Florida High Tech Corridor Matching Fund (FHT 09-18).

References

[1] N.S. Sariciftci, L. Smilowitz, A.J. Heeger, F. Wudl, Photoinduced electron transfer from a conducting polymer to buckminsterfullerene, Science 258 (1992) 1474–1476.
[2] G. Yu, J. Gao, J.C. Hummelen, F. Wudl, A.J. Heeger, Polymer photovoltaic cells: enhanced efficiencies via a network of internal donor–acceptor heterojunction, Science 270 (1995) 1789–1791.
[3] C.Y. Yang, A.J. Heeger, Morphology of composites of semiconducting polymers mixed with C_{60}, Synth. Met. 83 (1996) 85–88.
[4] S.E. Shaheen, C.J. Brabec, N.S. Sariciftci, F. Padinger, T. Fromherz, J.C. Hummelen, 2.5% efficient organic plastic solar cells, Appl. Phys. Lett. 78 (2001) 841–843.
[5] F. Padinger, R.S. Rittberger, N.S. Sariciftci, Effects of postproduction treatment on plastic solar cells, Adv. Funct. Mater. 13 (2003) 85–88.

[6] C.J. Brabec, S.E. Shaheen, C. Winder, N.S. Sariciftci, P. Denk, Effect of LiF/metal electrodes on the performance of plastic solar cells, Appl. Phys. Lett. 80 (2002) 1288–1290.
[7] W. Ma, C. Yang, X. Gong, K. Lee, A.J. Heeger, Thermally stable, efficient polymer solar cells with nanoscale control of the interpenetrating network morphology, Adv. Funct. Mater. 15 (2005) 1617–1622.
[8] M. Reyes-Reyes, K. Kim, D.L. Carroll, High-efficiency photovoltaic devices based on annealed poly(3-hexylthiophene) and 1-(3-methoxycarbonyl)-propyl-1- phenyl-(6,6)C61 blends, Appl. Phys. Lett. 87 (2005) 083506–083508.
[9] H.Y. Chen, J.H. Hou, S.Q. Zhang, Y.Y. Liang, G.W. Yang, Y. Yang, L.P. Yu, Y. Wu, G. Li, Polymer solar cells with enhanced open-circuit voltage and efficiency, Nat. Photonics 3 (2009) 649–653.
[10] (a) Frederik C. Krebs, Kion Norrman, Using light-induced thermocleavage in a roll-to-roll process for polymer solar cells, ACS Appl. Mater. Interfaces 2 (2010) 877–887;
(b) Frederik C. Krebs, Suren A. Gevorgyan, Jan Alstrup, A roll-to-roll process to flexible polymer solar cells: model studies, manufacture and operational stability studies, J. Mater. Chem. 19 (2009) 5442–5451;
(c) F.C. Krebs, H. Spanggard, T. Kjær, M. Biancardo, J. Alstrup, Large area plastic solar cell modules, Mater. Sci. Eng. B 138 (2007) 106–111.
[11] R. Steim, P. Schilinsky, S.A. Choulis, C.J. Brabec, Flexible polymer photovoltaic modules with incorporated organic bypass diodes to address module shading effects, Sol. Energy Mater. Sol. Cells 93 (2009) 1963–1967.
[12] L. Blankenburg, K. Schultheis, H. Schache, S. Sensfuss, M. Schrödner, Reel to reel wet coating as an effieicnt up-scaling techniue for the production of bulk-heterojunction polymer solar cells, Sol. Energy Mater. Sol. Cells 93 (2009) 476–483.
[13] M. Niggemann, B. Zimmermann, J. Haschke, M. Glatthaar, A. Gombert, Organic solar cell modules for specific applications—from energy autonomous systems to large area photovoltaics, Thin Solid Films 516 (2008) 7181–7187.
[14] R. Tipnis, J. Bernkopf, S. Jia, J. Krieg, S. Li, M. Storch, D. Laird, Large-area organic photovoltaic module—fabrication and performance, Sol. Energy Mater. Sol. Cells 93 (2009) 442–446.
[15] C. Lungenschmied, G. Dennler, H. Neugebauer, S.N. Sariciftci, M. Glatthaar, T. Meyer, A. Meyer, Flexible, long-lived, large-area, organic solar cells, Sol. Energy Mater. Sol. Cells 91 (2007) 379–384.
[16] Jae Woong Jung, Won Ho Jo, Annealing-free high efficiency and large area polymer solar cells fabricated by a roller painting process, Adv. Func. Mater. 20 (2010) 2355–2363.
[17] B. Zimmermann, M. Glatthaar, M. Niggemann, M.K. Riede, A. Hinsch, A. Gombert, ITO-free wrap through organic solar cells—a module concept for cost-efficient reel-to-reel production, Sol. Energy Mater. Sol. Cells 91 (2007) 374–378.
[18] Matthieu Manceau, Dechan Angmo, Mikkel Jørgensen, Frederik C. Krebs, ITO-free flexible polymer solar cells: from small model devices to roll-to-roll processed large modules, Org. Electron. 12 (2011) 566–574.
[19] Frederik C. Krebs, All solution roll-to-roll processed polymer solar cells free from indium-tin-oxide and vacuum coating steps, Org. Electron. 10 (2009) 761–768.
[20] (a) Jinsong Huang, Gang Li, Yang Yang, A Semi-transparent plastic solar cell fabricated by a lamination process, Adv. Mater. 20 (2008) 415–419;
(b) Bang-Ying Yu, Ating Tsai, Shu-Ping Tsai, Ken-Tsung Wong, Yang Yang, Chih-Wei Chu, Jing-Jong Shyue, Efficient inverted solar cells using TiO_2 nanotube arrays, Nanotechnology 19 (2008) 255202–255207;
(c) G. Li, C.-W. Chu, V. Shrotriya, J. Huang, Y. Yang, Efficient inverted polymer solar cells, Appl. Phys. Lett. 88 (2006) 253503–253506.
[21] Jingyu Zou, Hin-Lap Yip, Steven K. Hau, Alex K.-Y. Jen, Metal grid/conducting polymer hybrid transparent electrode for inverted polymer solar cells, Appl. Phys. Lett. 96 (2010) 203301–203304.
[22] C. Waldauf, M. Morana, P. Denk, P. Schilinsky, K. Coakley, S.A. Choulis, C.J. Brabec, High efficient inverted organic photovoltaics using solution based titanium oxide as electron selective contact, Appl. Phys. Lett. 89 (2006) 233517–233520.
[23] Y. Zhou, F. Li, S. Barrau, W. Tian, O. Inganas, F. Zhang, Inverted and transparent polymer solar cells prepared with vacuum-free processing, Sol. Eng. Sol. Cells 93 (2009) 497–500.
[24] Jonas Weickert, Haiyan Sun, Claudia Palumbiny, Holger Christian Hesse and Lukas Schmidt–Mende, spray-deposited PEDOT:PSS for inverted organic solar cells, Sol. Energy Mater. Sol. Cells 94 (2010) 2371–2374.
[25] Joon-Sung Kim, Won-Suk Chung, Kyungkon Kim, Dong Young Kim, Ki-Jung Paeng, Seong Mu Jo, Sung-Yeon Jang, Performance optimization of polymer solar cells using electrostatically sprayed photoactive layers, Adv. Funct. Mater. 20 (2010) 3538–3546.
[26] Kyu-Jin Kim, Yeong-Seon Kim, Jin-Uk Park, Won-Seok Kang, Byoung-Ho Kang, Se-Hyuk Yeom, Do-Eok Kim, Jae-Ho Kim, Shin-Won Kang, Substrate heated spray-deposition method for high efficient organic solar cell: morphology inspection, Jap. J. Appl. Phys. 49 (2010) 01800–01804.
[27] Y. Lim, S. Lee, D.J. Herman, M.T. Lloyd, J.F. Anthony, G.G. Malliaras, Spray-deposited poly(3.4-ethylenedioxythiophene):poly(styrenesulfonate) top electrode for organic solar cells, Appl. Phys. Lett. 93 (2008) 193301–193304.
[28] J. Lewis, J. Zhang, X. Jiang, Fabrication of organic solar array for applications in microelectromechanical systems, J. Renewable Sustainable Energy 1 (2009) 013101–013109.
[29] Peter Van Zant, Microchip Fabrication, McGraw-Hill, New York, ISBN 0-07-135636-3, 2000, pp. 431–2.
[30] L.J. van der Pauw, A method of measuring the resistivity and Hall coefficient on lamellae of arbitrary shape, Philips Tech. Rev. 20 (1958) 220–224.
[31] R.J. Kline, M.D. McGehee, Morphology and charge transport in conjugated polymers, J Macromol. Sci. C: Polym. Rev. 46 (2006) 27–45.
[32] Alain Geiser, Bin Fan, Hadjar Benmansour, Fernando Castro, Jakob Heier, Beat Keller, Mayerhofer, Karl Emanuel, Frank Nueesch, Roland Hany, Poly(3-hexylthiophene)/C_{60} heterojunction solar cells: implication of morphology on performance and ambipolar charge collection, Sol. Eng. Sol. Cells 92 (2008) 464–473.
[33] W. Graupner, G. Leditzky, G. Leising, U. Scherf, Shallow and deep traps in conjugated polymers of high intrachain order, Phys. Rev. B 54 (1996) 7610–7613.
[34] J. Nelson, Organic photovoltaic films, Curr. Opinion Solid State Mater. Sci. 6 (2002) 87–95.
[35] G. Dennler, C. Lungenschmied, H. Neugebauer, N.S. Sariciftci, M. Latrèche b, G. Czeremuszkin, M.R. Wertheimer, A new encapsulation solution for flexible organic solar cells, Thin Solid Films 511–512 (2006) 349–353.